LETTER

doi:10.1038/nature09933

Electromagnetically induced transparency and slow light with optomechanics

A. H. Safavi-Naeini[1]*, T. P. Mayer Alegre[1]*, J. Chan[1], M. Eichenfield[1], M. Winger[1], Q. Lin[1], J. T. Hill[1], D. E. Chang[2,3] & O. Painter[1]

Controlling the interaction between localized optical and mechanical excitations has recently become possible following advances in micro- and nanofabrication techniques[1,2]. So far, most experimental studies of optomechanics have focused on measurement and control of the mechanical subsystem through its interaction with optics, and have led to the experimental demonstration of dynamical back-action cooling and optical rigidity of the mechanical system[1,3]. Conversely, the optical response of these systems is also modified in the presence of mechanical interactions, leading to effects such as electromagnetically induced transparency[4] (EIT) and parametric normal-mode splitting[5]. In atomic systems, studies[6,7] of slow and stopped light (applicable to modern optical networks[8] and future quantum networks[9]) have thrust EIT to the forefront of experimental study during the past two decades. Here we demonstrate EIT and tunable optical delays in a nanoscale optomechanical crystal, using the optomechanical nonlinearity to control the velocity of light by way of engineered photon–phonon interactions. Our device is fabricated by simply etching holes into a thin film of silicon. At low temperature (8.7 kelvin), we report an optically tunable delay of 50 nanoseconds with near-unity optical transparency, and superluminal light with a 1.4 microsecond signal advance. These results, while indicating significant progress towards an integrated quantum optomechanical memory[10], are also relevant to classical signal processing applications. Measurements at room temperature in the analogous regime of electromagnetically induced absorption show the utility of these chip-scale optomechanical systems for optical buffering, amplification, and filtering of microwave-over-optical signals.

It is by now well known that the optical properties of matter can be dramatically modified by using a secondary light beam, approximately resonant with an internal process of the material system. As an example, an opaque object can be made transparent in the presence of a control beam; this is the phenomenon of EIT. A remarkable feature of EIT is the drastic reduction in the group velocity of light passing through the material, achieved inside a practically lossless transparency window. This aspect of the effect has been used in schemes whereby light may be slowed and stopped, making it an important building block in quantum information and communication proposals, as well as of great practical interest in classical optics and photonics. A simple upper-bound for the storage time in EIT-based proposals is the lifetime related to the internal processes of the material. These lifetimes can be extremely long in atomic gases, with storage times of the order of one second having been demonstrated[11] in Bose–Einstein condensates. Part of the vision for future scalable quantum networks has involved extending the remarkable results achieved in atomic experiments to a more readily deployable domain.

In the solid state, EIT has been demonstrated in quantum wells, dots and nitrogen–vacancy centres[12–14]. But the fast dephasing rates and inhomogeneous broadening of solid-state electronic resonances have led to a plethora of other methods and techniques. Elegant experiments with stimulated Brillouin scattering in fibres[15] and coherent population oscillations[16] have been used to delay intense classical light. Alternatively, for quantum storage and buffering, techniques related to photon-echo spectroscopy (for example, controllable reversible inhomogeneous broadening[17] and atomic frequency combs[18]) have been used successfully to achieve solid-state quantum memories. In chip-scale photonics, dynamically tunable arrays of cavities, displaying EIT, are an intriguing analogue to ensembles of atoms and provide a route to slowing and stopping light all-optically[19]. Generally, the elements in the arrays have consisted of coupled optical or plasmonic resonances, and have been demonstrated with couplings engineered to give rise to Fano-like interference[20]. However, a significant limitation in these all-photonic systems is the short optical resonance lifetime. We demonstrate here that in addition to optically controlled switching of a probe beam, as recently presented by others[4], EIT in an optomechanical cavity may be used to change the group velocity of light significantly. As such, tunable optical delay, with delay times limited by the much longer mechanical resonance lifetime of the optomechanical system, may be achieved. These delays are also attainable across a broad spectrum of wavelengths; indeed, recent circuit cavity electromechanics experiments in the strong-coupling regime have demonstrated EIT and group velocity control at microwave frequencies[21]. Additionally, the ability to create arrays of coupled devices by 'printing' optomechanical circuits onto a Si microchip[22–24], for example, allows one to create a much larger delay-bandwidth product (scaling as $\sqrt{N}$, N being the number of cavity elements)[10]; such arrays provide a means to sample an incoming optical pulse shape, store it and retrieve it, much like an ensemble of atoms does in atomic EIT.

EIT in optomechanical systems can be understood physically as follows. The conventional radiation pressure interaction between a near-resonant cavity light field and mechanical motion is modelled by the nonlinear Hamiltonian $H_{\rm int}=\hbar g\hat{a}^{\dagger}\hat{a}\left(\hat{b}+\hat{b}^{\dagger}\right)$. Here $\hat{a}$ ($\hat{a}^{\dagger}$) and $\hat{b}$ ($\hat{b}^{\dagger}$) are the annihilation (creation) operators of photon and phonon resonator quanta, respectively, g is the optomechanical coupling rate corresponding physically to the shift in the optical mode's frequency due to the zero-point fluctuations of the phonon mode, and $\hbar$ is $h/2\pi$, where h is Planck's constant. By driving the system with an intense red-detuned optical 'control' beam at frequency $\omega_{\rm c}$, as shown in Fig. 1a, the form of the effective interaction changes (in the resolved sideband limit) to that of a beam-splitter-like Hamiltonian, $H_{\rm int}=\hbar G\left(\hat{a}^{\dagger}\hat{b}+\hat{a}\hat{b}^{\dagger}\right)$. Here, the zero-point-motion coupling rate g is replaced by a much stronger parametric coupling rate $G=g\sqrt{\langle n_{\rm c}\rangle}$ between light and mechanics, where $\langle n_{\rm c}\rangle$ is the stored intracavity photon number induced by the control beam. Viewed in a dressed-state picture, with the control beam detuning from the optical cavity resonance ($\omega_{\rm o}$) set equal to the mechanical frequency ($\omega_{\rm m}$), $\Delta_{\rm OC}\equiv\omega_{\rm o}-\omega_{\rm c}\approx\omega_{\rm m}$, the optical and mechanical modes $\hat{a}$ and $\hat{b}$ become coupled (denoted $\hat{a}_{\rm d}$ and $\hat{b}_{\rm d}$ in Fig. 1b). The dressed mechanical mode, now effectively a phonon–photon polariton, takes on a weakly photonic nature, coupling it to the optical loss channels at a rate $\gamma_{\rm om}\equiv C\gamma_{\rm i}$, where the optomechanical

[1]Thomas J. Watson Sr Laboratory of Applied Physics, California Institute of Technology, Pasadena, California 91125, USA. [2]Institute for Quantum Information, California Institute of Technology, Pasadena, California 91125, USA. [3]Center for the Physics of Information, California Institute of Technology, Pasadena, California 91125, USA.
*These authors contributed equally to this work.

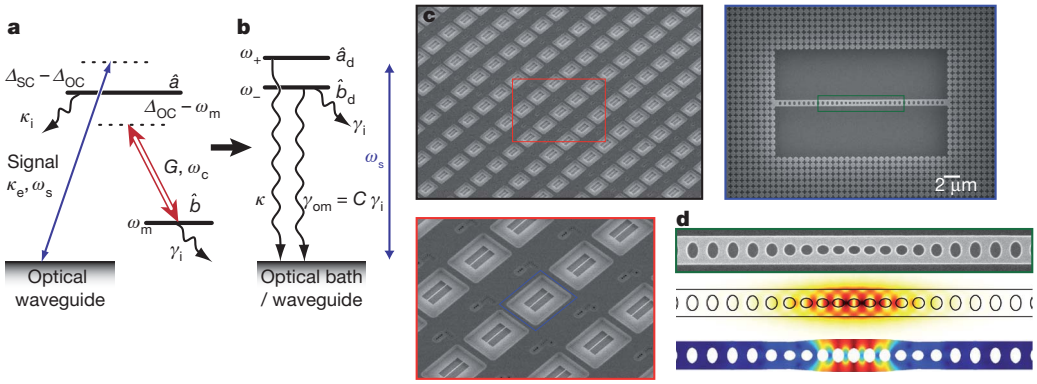

Figure 1 | Optomechanical system. **a**, Level-diagram picture, showing three 'levels' that represent the optical mode $\hat{a}$, the mechanical mode $\hat{b}$ and the 'bath' of optical waveguide modes. The transitions between modes driven by the signal and control beams are indicated by blue and red double-headed arrows, respectively. Wavy black arrows indicate decay from the different modes. See text for definitions of symbols in **a** and **b**. **b**, The control beam at ω_c drives the transition between the optical and mechanical mode, dressing the optical and mechanical modes, resulting in the dressed state picture with dressed modes $\hat{a}_d$ and $\hat{b}_d$. **c**, Series of scanning electron micrographs, showing large array of optomechanical crystal nanocavities (top-left panel), zoomed-in image of device array (bottom-left panel), and zoomed-in image of top-view of single cavity device (top-right panel). **d**, From top to bottom: scanning electron micrograph of a zoomed-in region showing the OMC defect region; finite-element-method (FEM) simulation results for the optical field showing the electrical field intensity $|\mathbf{E}(\mathbf{r})|$; FEM-simulated mechanical mode with the total displacement $|\mathbf{Q}(\mathbf{r})|$ shown.

cooperativity is defined as $C \equiv 4G^2/\kappa\gamma_i$ for an optical cavity decay rate of κ, and an intrinsic mechanical resonance damping rate of γ_i.

The drive-dependent loss rate γ_{om} has been viewed in most previous studies as an incoherent, quantum-limited loss channel, and was used in recent experiments to cool the mechanical resonator close to its quantum ground state[25]. In the dressed mode picture, by analogy to the dressed state view of EIT[7], it becomes clear that a coherent cancellation of the loss channels in the dressed optical and mechanical modes is possible, and can be used to switch the system from absorptive to transmittive in a narrow band around cavity resonance. Much as in atomic EIT, this effect causes an extremely steep dispersion for the transmitted probe photons, with a group delay on resonance of (see Supplementary Information)

$$\tau^{(T)}\big|_{\omega=\omega_m} = \frac{2}{\gamma_i}\frac{(\kappa_e/\kappa)C}{(1+C)(1-(\kappa_e/\kappa)+C)} \qquad (1)$$

where κ_e is the optical coupling rate between the external optical waveguide and the optical cavity, and the delay is dynamically tunable via the control beam intensity through C.

Nano- and micro-optomechanical resonators take a variety of forms, among which optomechanical crystals (OMC) have been used to demonstrate large radiation-pressure-induced interaction strengths between gigahertz mechanical resonances and near-infrared optical resonances[24]. The nanobeam OMC cavity used in this study (Fig. 1c and d) uses a periodic free-standing Si structure to create high-Q co-localized optical and mechanical resonances. These devices can be printed and etched into the surface of a Si chip in large arrays (Fig. 1c), and are designed to operate optically in the telecommunications band ($\lambda_o = 1{,}550$ nm) and acoustically at microwave frequencies ($\omega_m/2\pi = 3.75$ GHz). The theoretical optomechanical coupling rate g between co-localized photon and phonon modes is $g/2\pi \approx 800$ kHz. By optimizing the arrangement of holes in the central cavity region of the nanobeam where light and sound are localized, an intrinsic optical decay rate of $\kappa_i/2\pi \approx 290$ MHz is obtained for the optical cavity mode, placing the optomechanical system in the resolved sideband regime ($\omega_m/\kappa_i \gg 1$) necessary for EIT. The corresponding mechanical resonance is measured to have an intrinsic damping rate of $\gamma_i/2\pi \approx 250$ kHz at temperature $T = 8.7$ K, corresponding to a mechanical Q-factor of $Q_m = 15{,}000$. Light is coupled into and out of the device using a specially prepared optical fibre taper, which when placed in the near-field of the nanobeam cavity couples the guided modes of the taper evanescently to the optical resonances of the nanobeam (see Supplementary Information for details of the optical cavity loading).

In order to characterize the near-resonance optical reflection of the cavity system, a sideband of the control beam is created using electro-optic modulation (see Methods and Supplementary Information), forming a weak signal beam with tunable frequency ω_s. The results of measurements performed at a cryogenic temperature of 8.7 K are shown in Fig. 2. Here, the control beam laser power was varied from 6 μW ($\langle n_c \rangle = 25$) to nearly 250 μW ($\langle n_c \rangle = 1{,}040$). The frequencies of both the control and signal beams are swept in order to map out the system dependence on control beam detuning, Δ_{OC}, and the two-photon detuning, $\Delta_{SC} = \omega_s - \omega_c$. The resulting reflected optical signal intensity, separated from the control beam via a modulation and lock-in technique (see Methods and Supplementary Information), is shown in Fig. 2a for a series of control laser detunings. Visible in each of the plots is a broad resonance corresponding to the bare optical cavity response with loaded linewidth $\kappa/2\pi \approx 900$ MHz. A much narrower reflection dip feature, corresponding to the transparency window, can also be seen near the cavity line centre. The position of the narrow reflection dip tracks with a two-photon detuning equal to the mechanical resonance frequency, $\Delta_{SC} \approx \omega_m$. This region is shown in more detail in Fig. 2b, where the Fano-like structure of the optical response is apparent. Each curve in Fig. 2a and b is a horizontal slice of the data presented in Fig. 2c, where the reflectivity is plotted as a function of both ω_c and Δ_{SC}. The transparency window is shown to be fully controllable via the applied light field, the window expanding and contracting with the control beam laser power (Fig. 2d and e). At the maximum stable control power (unstable regions due to a thermo-optic bistability induced by optical absorption are shown as hatched regions in Fig. 2c), a transparency window approaching 5 MHz is obtained.

Model fits to the reflection spectra (see Supplementary Information) are shown as solid curves in Fig. 2a and b. The resulting fitted values for $\gamma_{om} = 4G^2/\kappa$ for each control power are shown in Fig. 2e. A linear fit to the extracted data yields a value for the zero-point-motion coupling constant of $g/2\pi = 800$ kHz, in agreement with the value obtained from independent optical transduction measurements of the thermal Brownian motion of the mechanical oscillator[24]. In addition to the intensity response of the optomechanical cavity there is the phase response, which provides a measure of the group delay of the modulated optical signal beam as it passes through the cavity. For the 89-kHz modulation of the signal beam used in our experiments, corresponding to a free-space signal wavelength of ~3.4 km, phase shifts between the modulation sidebands and the signal carrier on the order of a fraction of a radian are measured in the region where Δ_{SC} is within a

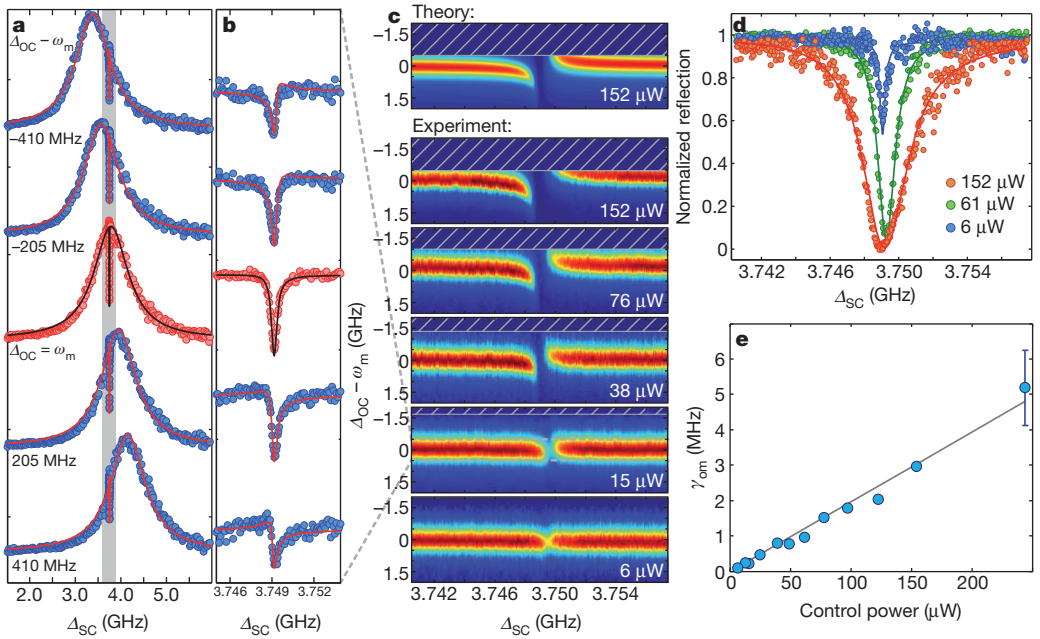

Figure 2 | Optical reflection response at temperature $T = 8.7$ K. a, Measured normalized reflection (dots) of the signal beam as a function of the two-photon detuning (Δ_{SC}) for a control beam power of 15 μW. **b**, Zoom-in of the reflected signal about the transparency window. Each spectrum in **a** and **b** corresponds to a different control laser detuning ($\Delta_{OC} - \omega_m$) as indicated. Solid curves correspond to model fits to the data (see Supplementary Information). **c**, Intensity plots for the signal beam reflection as a function of both control laser detuning (Δ_{OC}) and two-photon detuning (Δ_{SC}) for a series of different control beam powers (as indicated). The hatched areas are unstable regions for the control laser detuning at the given input power. The top plot is the theoretically predicted reflection spectrum for the highest control beam power. **d**, Transparency window versus control beam power for control laser detuning $\Delta_{OC} \approx \omega_m$. **e**, Transparency window bandwidth ($\gamma_{om} = 4G^2/\kappa$) versus control beam power (error bars indicate the standard deviation in the fit of γ_{om} to the EIT intensity spectra versus Δ_{OC}). The solid line represents the bandwidth scaling for a single best-fit value of $g/2\pi = 800$ kHz.

mechanical linewidth of ω_m. The measured phase-shifts for the reflected signal beam correspond to advances in time of the modulated signal, pointing to causality-preserving superluminal effects. A plot of the peak effective signal advance versus control beam power is plotted in Fig. 3a, ascertained from a fit to the reflection phase response spectra (Fig. 3b). For the highest control power, the reflected signal is advanced by 1.3 μs, roughly 7,000 times longer than the bare optical cavity lifetime.

The delay in transmission is directly related to the advance on reflection through the bare cavity transmission contrast (measured independently; see Supplementary Information). As such, we plot the corresponding transmission group delay of the signal in Fig. 3c. The theoretical delay/advance of the modulated signal beam for system parameters given by fits to the EIT intensity spectra are shown as dashed curves in Fig. 3a and c, indicating good agreement with the measured phase response. As can be seen in these data, the maximum measured transmission delay is $\tau^{(T)} \approx 50$ ns, which—although corresponding to significant slowing of light (to a velocity of $v_g \approx 40\ \mathrm{m\ s^{-1}}$) through the few-micrometre-long structure—is much smaller than the measured reflected signal advance or the limit set by the intrinsic mechanical damping ($2/\gamma_i \approx 1.4$ μs). This is due to the weak loading of the optical cavity in these experiments (see Supplementary Information), and the resulting small fraction of transmitted light that actually passes through the cavity.

In addition to the observed EIT-like behaviour of the optomechanical system, a similar phenomena to that of electromagnetically induced absorption (EIA)[26] in atomic systems can be realized by setting the detuning of the control beam to the blue side of the optomechanical cavity resonance ($\Delta_{OC} < 0$). Under blue-detuned pumping, the effective Hamiltonian for the optical signal and mechanical phonon mode becomes one of parametric amplification, $H_{int} = \hbar G\left(\hat{a}^\dagger \hat{b}^\dagger + \hat{a}\hat{b}\right)$. The measured reflection spectrum from the OMC is shown in Fig. 3d, where the reflectivity of the cavity system is seen to be enhanced around the two-photon detuning $\Delta_{SC} \approx \omega_m$, a result of the increased 'absorption' (feeding) of photons into the cavity. As discussed further in the Supplementary Information, at even higher control beam powers such that $C \gtrsim 1$, the system switches from EIA to parametric amplification, resulting in optical signal amplification, and eventually phonon-lasing.

Reflection spectroscopy at room temperature (296 K) of the optomechanical cavity has also been performed (presented in Supplementary Information), and yields similar results to that of the cryogenic measurements, albeit with a larger value of $\langle n_c \rangle$ required to reach a given cooperativity (see Fig. 3e) owing to the larger intrinsic mechanical dissipation at room temperature ($\gamma_i = 2\pi \times 1.9$ MHz). Beyond the initial demonstrations of EIT and EIA behaviour in the OMC cavities presented here, it is fruitful to consider the bandwidth and signal delay limits that might be attainable with future improvements in device material or geometry. For instance, the transparency bandwidth of the current devices is limited by two-photon absorption of the control beam in the silicon cavities; a move to larger-bandgap dielectric materials, such as silicon nitride, should allow intra-cavity photon numbers of 10^6 (limited by linear material absorption), resulting in a transparency window approaching $G = g\sqrt{\langle n_c \rangle} \approx 2\pi(1\ \mathrm{GHz})$. Also, recent research into low-loss GHz mechanic resonators[27] should enable slow light optical delays approaching 10 μs at room temperature, roughly equivalent to the optical path length of a kilometre of optical fibre. Much like the acoustic wave devices used in electronic systems[28], optomechanical devices with these attributes would enable chip-scale microwave photonic systems capable of advanced signal processing in the optical domain, such as that needed for emerging broadband wireless access networks or more specialized applications, such as true-time delays in radar systems[8].

The limiting factor for quantum applications of optomechanical systems is the re-thermalization time of the mechanical resonator, $\tau_{th} = \hbar Q_m/kT$, which in the case of a quantum optical memory

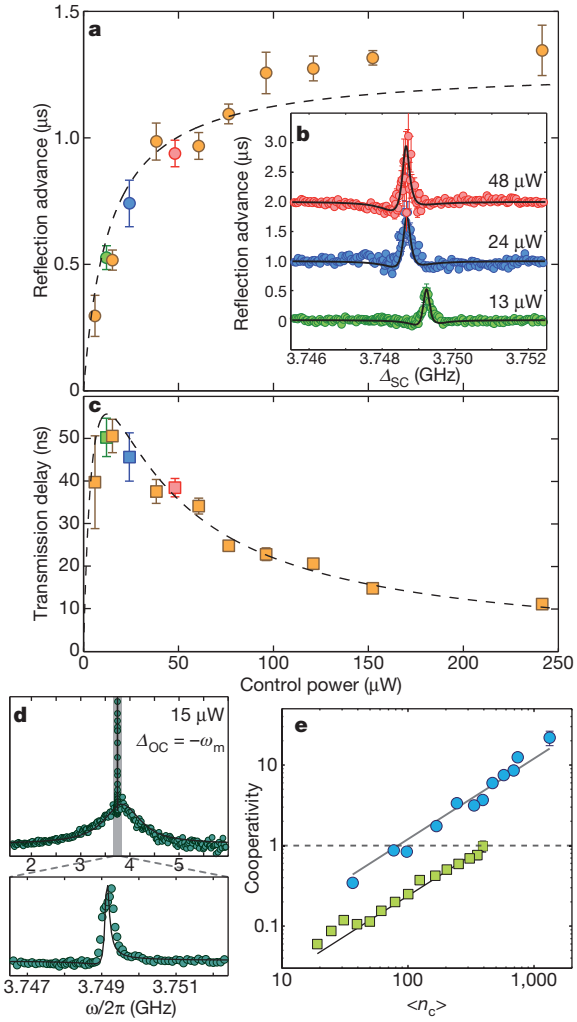

Figure 3 | Measured temporal shifts and amplification. **a**, Maximum measured reflected signal advance as a function of the control beam power. **b**, Measured reflected signal advance versus two-photon detuning, Δ_{SC}. Solid curves correspond to fit from model (see Supplementary Information). Curves at different control powers are shifted for clarity. **c**, Inferred maximum transmitted signal delay versus control beam power. Dashed lines in **a** and **c** are theoretical advance/delay times predicted from model of optomechanical system based on intensity response of the optomechanical system. **d**, Measured signal reflection as a function of two-photon detuning for the control laser blue-detuned from the cavity. **e**, Measured cooperativity for sample temperature of 296 K (squares) and 8.7 K (circles) as a function of the average number of control photons inside the cavity. Error bars indicate the standard deviation in the model fit to the EIT spectral data at each control beam power.

represents the average storage time of a single photon before excitation of the system by a thermal bath phonon. For the devices studied here, despite the optical cooling and reduced phonon occupancy of the mechanical resonator provided by the control beam (the cooling rate being equal to the transparency window bandwidth[10]), the re-thermalization time is limited to $\tau_{th} \approx 12$ ns by the 8.7 K bath temperature. Reducing the operating temperature further to a value below 100 mK (routinely attained in a dilution refrigerator) would not only increase the re-thermalization time through a lower bath temperature, but should also result in a significant increase in the mechanical Q-factor. Taken together, the resulting re-thermalization time in the current OMC devices at $T = 100$ mK is likely to be of the order of 100 μs, which although not nearly as long as what has been achieved in atomic systems[11], still represents a substantial storage time compared to the realizable GHz bandwidth of the system. Additionally, optomechanical processes similar to the EIT behaviour measured here have also been proposed[29,30] to provide an optical interface between, for instance, atomic and superconducting circuit quantum systems, enabling the formation of hybrid quantum networks.

METHODS SUMMARY

Fabrication. The nanobeam cavities were fabricated using a silicon-on-insulator wafer from SOITEC (resistivity $\rho = 4$–$20\ \Omega$ cm, device layer thickness $t = 220$ nm, buried-oxide layer thickness 2 μm). The cavity geometry is defined by electron beam lithography followed by inductively-coupled-plasma reactive ion etching to transfer the pattern through the 220-nm silicon device layer. The cavities were then undercut using an HF:H_2O solution to remove the buried oxide layer, and cleaned using a piranha etch/HF etch cycle. The dimensions and design of the nanobeam will be discussed in detail elsewhere.

Experimental set-up. We demonstrate EIT via reflection measurements of the optically pumped system at varying $\langle n_c \rangle$. Using the experimental set-up shown in Supplementary Information, a laser beam at ω_c (the control beam) is sent through an electro-optical modulator with drive frequency equal to Δ_{SC}, creating an optical sideband at frequency ω_s (the signal beam), which is amplitude modulated at $\omega_{LI}/2\pi = 89$ kHz. Since the control beam is detuned from the cavity by $|\Delta_{OC}| \gg \kappa$, it is effectively filtered when looking in reflection, while the modulated signal beam at $\omega_c \pm \Delta_{SC}$ (where the sign is that of Δ_{OC}) is near resonance with the optical cavity and is reflected. The reflected signal beam is detected using a 12-GHz New Focus PIN photo-diode, with the output electrical signal sent to a lock-in amplifier where the component related to the modulated tone ($\omega_{LI} = 89$ kHz) is amplified and sent to an oscilloscope. By scanning both the laser frequency ω_c and the two-photon detuning Δ_{SC}, a full map of the reflectivity is obtained. Additionally, by using a lock-in amplifier, the phase of the modulated signal sidebands relative to the carrier can be measured, giving a direct measurement of the group delay imparted on the optical signal beam by the optomechanical cavity.

Received 8 December 2010; accepted 21 February 2011.
Published online 16 March 2011.

1. Kippenberg, T. J. & Vahala, K. J. Cavity optomechanics: back-action at the mesoscale. *Science* **321,** 1172–1176 (2008).
2. Favero, I. & Karrai, K. Optomechanics of deformable optical cavities. *Nature Photon.* **3,** 201–205 (2009).
3. Braginsky, V. B. *Measurement of Weak Forces in Physics Experiments* (Univ. Chicago Press, 1977).
4. Weis, S. *et al.* Optomechanically induced transparency. *Science* **330,** 1520–1523 (2010).
5. Gröblacher, S., Hammerer, K., Vanner, M. & Aspelmeyer, M. Observation of strong coupling between a micromechanical resonator and an optical cavity field. *Nature* **460,** 724–727 (2009).
6. Hau, L. V., Harris, S. E., Dutton, Z. & Behroozi, C. H. Light speed reduction to 17 metres per second in an ultracold atomic gas. *Nature* **397,** 594–598 (1999).
7. Fleischhauer, M., Imamoglu, A. & Marangos, J. P. Electromagnetically induced transparency: optics in coherent media. *Rev. Mod. Phys.* **77,** 633–673 (2005).
8. Boyd, R. W. & Gauthier, D. J. Controlling the velocity of light pulses. *Science* **326,** 1074–1077 (2009).
9. Kimble, H. J. The quantum internet. *Nature* **453,** 1023–1030 (2008).
10. Chang, D., Safavi-Naeini, A. H., Hafezi, M. & Painter, O. Slowing and stopping light using an optomechanical crystal array. *N. J. Phys.* **13,** 023003 (2011).
11. Zhang, R., Garner, S. R. & Hau, L. V. Creation of long-term coherent optical memory via controlled nonlinear interactions in Bose-Einstein condensates. *Phys. Rev. Lett.* **103,** 233602 (2009).
12. Phillips, M. C. *et al.* Electromagnetically induced transparency in semiconductors via biexciton coherence. *Phys. Rev. Lett.* **91,** 183602 (2003).
13. Santori, C. *et al.* Coherent population trapping of single spins in diamond under optical excitation. *Phys. Rev. Lett.* **97,** 247401 (2006).
14. Xu, X. *et al.* Coherent population trapping of an electron spin in a single negatively charged quantum dot. *Nature Phys.* **4,** 692–695 (2008).
15. Thévenaz, L. Slow and fast light in optical fibres. *Nature Photon.* **2,** 474–481 (2008).
16. Bigelow, M. S., Lepeshkin, N. N. & Boyd, R. W. Superluminal and slow light propagation in a room-temperature solid. *Science* **301,** 200–202 (2003).
17. Afzelius, M., Simon, C., de Riedmatten, H. & Gisin, N. Multimode quantum memory based on atomic frequency combs. *Phys. Rev. A* **79,** 052329 (2009).
18. de Riedmatten, H., Afzelius, M., Staudt, M. U., Simon, C. & Gisin, N. A solid-state light-matter interface at the single-photon level. *Nature* **456,** 773–777 (2008).
19. Yanik, M. F., Suh, W., Wang, Z. & Fan, S. Stopping light in a waveguide with an all-optical analog of electromagnetically induced transparency. *Phys. Rev. Lett.* **93,** 233903 (2004).
20. Xu, Q. *et al.* Experimental realization of an on-chip all-optical analogue to electromagnetically induced transparency. *Phys. Rev. Lett.* **96,** 123901 (2006).
21. Teufel, J. D. *et al.* Circuit cavity electromechanics in the strong coupling regime. *Nature* doi:10.1038/nature09898 (10 March 2011); preprint at ⟨http://arXiv.org/abs/1011.3067⟩ (2010).
22. Notomi, M., Kuramochi, E. & Tanabe, T. Large-scale arrays of ultrahigh-Q coupled nanocavities. *Nature Photon.* **2,** 741–747 (2008).

23. Li, M. *et al.* Harnessing optical forces in integrated photonic circuits. *Nature* **456,** 480–484 (2008).
24. Eichenfield, M., Chan, J., Camacho, R. M., Vahala, K. J. & Painter, O. Optomechanical crystals. *Nature* **462,** 78–82 (2009).
25. Rocheleau, T. *et al.* Preparation and detection of a mechanical resonator near the ground state of motion. *Nature* **463,** 72–75 (2010); published online 9 December 2009.
26. Lezama, A., Barreiro, S. & Akulshin, A. M. Electromagnetically induced absorption. *Phys. Rev. A* **59,** 4732–4735 (1999).
27. Nguyen, C. T.-C. MEMS technology for timing and frequency control. *IEEE Trans. Ultrason. Ferroelectr. Freq. Control* **54,** 251–270 (2007).
28. Lakin, K., Kline, G. & McCarron, K. Development of miniature filters for wireless applications. *IEEE Trans. Microwave Theory Techn.* **43,** 2933–2939 (1995).
29. Stannigel, K., Rabl, P., Srensen, A. S., Zoller, P. & Lukin, M. D. Optomechanical transducers for long-distance quantum communication. *Phys. Rev. Lett.* **105,** 220501 (2010).
30. Safavi-Naeini, A. H. & Painter, O. Proposal for an optomechanical traveling wave phonon-photon translator. *N. J. Phys.* **13,** 013017 (2011).

Supplementary Information is linked to the online version of the paper at www.nature.com/nature.

Acknowledgements We thank K. Schwab for providing the microwave modulation source used in this work. This work was supported by the DARPA/MTO ORCHID programme through a grant from AFOSR, and the Kavli Nanoscience Institute at Caltech. A.H.S.-N. and J.C. acknowledge support from NSERC.

Author Contributions J.C., A.H.S.-N. and M.E. performed the device design, and J.C. performed the device fabrication with support from M.W. and J.T.H. Measurements and data analysis were performed by A.H.S.-N. and T.P.M.A., with support from both D.E.C. and Q.L. and supervision by O.P. All authors contributed to the writing of the manuscript.

Author Information Reprints and permissions information is available at www.nature.com/reprints. The authors declare no competing financial interests. Readers are welcome to comment on the online version of this article at www.nature.com/nature. Correspondence and requests for materials should be addressed to O.P. (opainter@caltech.edu).